**Fuel Cells**

# Inductive Low-Frequency Processes in PEMFC-Impedance Spectra▲

A. Schiefer[1]*, M. Heinzmann[1], A. Weber[1]

[1] Institute for Applied Materials (IAM-WET), Karlsruhe Institute of Technology (KIT), Adenauerring 20b, 76131 Karlsruhe, Germany

## Abstract

Impedance spectra of polymer electrolyte membrane (PEM) fuel cells often comprise an ''inductive loop'' at low frequencies from 1 Hz to 1 mHz additionally to the typically polarization resistances with capacitive behavior between 1 MHz to 1 Hz. To investigate this inductive behavior, systematic variations of operating parameters as humidity, current density and gas compositions are performed. The impedance spectra, including their inductive parts, are deconvoluted by an extended version of the distribution of relaxation times (DRT). Two inductive processes are identified in the DRT and subsequently quantified by fitting the spectra to an extended equivalent circuit model exhibiting negative resistances and constant phase elements.

Both inductive processes are depending on relative humidity and current density. The inductive behavior seems to be dominated by the oxygen reduction reaction (ORR) at the cathode, whereas changes in membrane hydration can be excluded as the main cause for the inductive low-frequency processes. Measurements in symmetrical $H_2/H_2$ operating mode prove that the inductive behavior cannot be solely related to the ORR.

The ratio of the inductive processes to the ohmic and capacitive loss processes ranges from 15% to 30%. Thus, a considerable cell performance improvement related to the existence of these inductive low-frequency processes has to be taken into account.

**Keywords:** Distribution of Relaxation Times, Electrochemical Characterization, Electrochemical Impedance Spectroscopy, Inductive Phenomena, PEMFC, Polymer Electrolyte Membrane Fuel Cell

## 1 Introduction

The profound understanding of the physicochemical origin and impact of the individual loss processes controlling the cell performance of polymer electrolyte membrane fuel cells (PEMFCs) is essential for a continuous further development. Still not all loss processes are fully understood and therefore require a detailed analysis. Electrochemical impedance spectroscopy (EIS) is a well-established characterization method for electrochemical systems, such as fuel cells. The impedance spectra of PEMFCs often comprise an "inductive loop" at frequencies <1 Hz additionally to ohmic and polarization resistances with capacitive behavior. For this loop, literature gives a variety of explanations, i.e., side reactions and reaction intermediates in oxygen reduction reaction as well as formation of platinum oxide and subsequent platinum dissolution [1–3]. Another prominent explanation is the water transport charac-

teristic and the related change in membrane hydration [3–5]. An overview over the explanations given in literature can be found in [6]. The consideration of such an effect in a physicochemical impedance model results in an "inductive" loop. So far, in most papers only one of the abovementioned effects is considered and the inductive loop is fully attributed to this effect.

In order to investigate the causes of this low frequency behavior a systematic variation of operating parameters (current density, relative humidity, potential, oxygen partial pressure) was performed. The method of the distribution of relaxation times (DRT) [7] was extended and applied to deconvolute the entire impedance spectrum and determine the corresponding time constants of the low-frequency processes. With this approach two different simultaneously occurring processes, one dominant at high potentials and one dominant at low humidity could be determined.

[*] *Corresponding author, anne.schiefer@kit.edu*

## 2 Experimental

### 2.1 Cell, Housing, and Test Bench

In this study, commercial membrane electrode assemblies (MEA) of type Greenerity® H500EL2 with a platinum loading of $0.4\,mg_{Pt}\,cm^{-2}$ (cathode) and $0.2\,mg_{Pt}\,cm^{-2}$ (anode), respectively, have been investigated. Single cells with an active surface area of 1 $cm^2$ were assembled between the gas diffusion layers (GDL 29 BC from SGL®) and placed into an in-house developed fuel cell housing. The contacting of the active electrode area is realized by gold flow fields with parallel flow channels (cross-section: 1 mm × 1 mm). The housing is compressed by stainless steel heat exchanger plates flowed by a thermal fluid. The cell temperature is controlled by a Julabo F32-ME thermostat. In this setup the GDL contact pressure is independent from sealing pressure and continuously adjustable from 0 to 200 N. All following measurements have been conducted by applying a contact pressure of 50 N, which correlates to 1 MPa with respect to the land area of the flow field. Mass flow controllers supply the gas in a well-defined mixture of oxygen, nitrogen and hydrogen to anode and cathode. The humidity in oxidant and fuel is generated in catalytic burner chambers ahead of the cell by reacting hydrogen and oxygen.

The combination of small active electrode areas, high gas flow rates and a parallel flow field structure eliminates lateral gradients in temperature, gas composition and current density. Thus, we reach homogenous operational states over the entire cell area. Further details about the cell and the test setup can be found in [8].

### 2.2 Measurement Techniques

Impedance spectra were recorded using a Zahner® Zennium E electrochemical workstation. To avoid unsteady conditions, the cell was stabilized for 90 min before each measurement. Linearity was assured by choosing a perturbation amplitude of 12 mV within a frequency range from 1 MHz down to 5 mHz (pseudo-galvanostatic mode). The lower frequency limit of 5 mHz was selected as a compromise between a full coverage of the inductive processes and instabilities during very long impedance measurement durations. For all impedance measurements 12 steps per decade and 20 measuring periods for frequencies above 66 Hz and 6 steps per decade and 10 measuring periods for frequencies below 66 Hz were chosen. These settings lead to a measurement duration of 2 h per impedance spectrum.

Flow rates of reactants were kept constant at $200\,mL\,min^{-1}$ leading to high stoichiometry ($\lambda > 10$). The cell was operated at ambient pressure and the cell temperature was held constant at 80 °C during all measurements. To investigate the dependencies of the inductive low-frequency processes, variations of relative humidity (30–70% R.H.) and current density (0–1.0 A cm$^{-2}$) were performed.

Unless otherwise mentioned the cell is supplied by hydrogen at the anode and pure oxygen at the cathode, both humi-dified at the same relative humidity level. Additionally, symmetrical $H_2/H_2$ measurements were performed, supplying similar amounts of humidified hydrogen to both electrodes. Bottled gases, provided by Air Liquide, with a purity of 99.95% ($O_2$), 99.9% ($H_2$) and 99.999% ($N_2$) were employed. For the humidification, steam was generated by reacting $O_2$ and $H_2$ in a burner-unit ahead of the cell. The given gas flow rate corresponds to the amount of humidified gas.

## 3 Impedance Data Analysis

### 3.1 Kramers-Kronig Validity Test

The distribution of relaxation times (DRT) analysis requires an outstanding impedance data quality since small deviation or single faulty measurement points can lead to misinterpretation and erroneous assignment of electrochemical processes [9]. To ensure the validity of impedance spectra a Kramers-Kronig test was performed [10]. All measured spectra were analyzed according to the method described in [11]. The impedance data is considered to fulfill the Kramers-Kronig relations, if the relative residuals do not exceed a value of 1%. This criterion was fulfilled by all spectra over the entire frequency range from 5 mHz to 1 MHz. It should be pointed out, that the low frequency parts of the spectra forming the "inductive loop" fulfilled the Kramers-Kronig test as well.

### 3.2 Distribution Function of Relaxation Times

The distribution of relaxation times (DRT) allows the identification and deconvolution of polarization processes with respect to their characteristic time constants without any previous model assumptions. This is especially advantageous when the exact number of polarization processes and their contribution to the total impedance is not known. The idea is to represent an impedance function which fulfills the Kramers-Kronig relations by an infinite number of infinitesimal differential RC-elements [12]. The mathematical relation between the distribution function $g(\tau)$ and the complex impedance $Z(\omega)$ is given by [12]:

$$Z(\omega) = R_0 + R_{pol} \int_0^\infty \frac{g(\tau)}{1 + j\omega\tau} d\tau \qquad (1)$$

In Eq. (1), $R_0$ represents the ohmic resistance and $R_{pol}$ the polarization resistance of the impedance data. To calculate the DRT of the measured spectra an approach based on the Tikhonov regularization [13] has been used [7,14].

Commonly, the DRT is only considering positive resistance and time constant values and thus is only able to account for capacitive processes. To include the "inductive loop" the DRT-calculation procedure had to be adapted. To account for the pseudo-inductive behavior observed in the spectra different approaches for the DRT-calculation are possible, as (i) include inductivities (i.e., RL-elements in addition to RC-elements) or (ii) allow negative resistance and capacity values.

# Fuel Cells

The different approaches were tested and it was found that inductivities (i) can hardly reproduce the measured spectra and the obtained inductivity values are physicochemically meaningless. A negative resistance and capacity (ii) in combination with the related time constant is corresponding to the physicochemically meaningful resistance decay due to an increase in current density. As pointed out in [15], such current-related resistance decay corresponds to a slow decrease of an ohmic or polarization resistance contribution. Thus, the inductive process leads to a "delayed" improvement in cell performance with a delay time corresponding to the relaxation frequency of the process.

If negative resistance values are enabled in the DRT calculation over the entire frequency range, additional (minor) negative peaks will appear at higher frequencies as well. This behavior has to be attributed to the Tikhonov regularization in combination with unavoidable noise in the measured data. The DRT will include such arbitrary negative peaks to achieve the smoothest solution. As a result, more peaks will appear and the area under the positive peaks does no longer correspond to the related polarization process. To avoid such instable and erroneous solutions the negative resistance values were limited to low frequencies starting slightly above the frequency with the first impedance value exhibiting a positive imaginary part (~140 mHz).

Figure 1a displays the Nyquist plot of a measured spectrum. The inductive loop at low frequencies is clearly visible. In Figure 1b the imaginary part as well as the DRT, calculated according to the method described above, is shown. The DRT deconvolutes two inductive and three capacitive processes. The capacitive processes at frequencies above 1 Hz, which were attribute to gas diffusion, charge transfer and ionic conduction in the ionomer [8], are not in the focus of this work. From the DRT it is obvious that there are at least 2 processes (peaks) $P_{ind,1}$ and $P_{i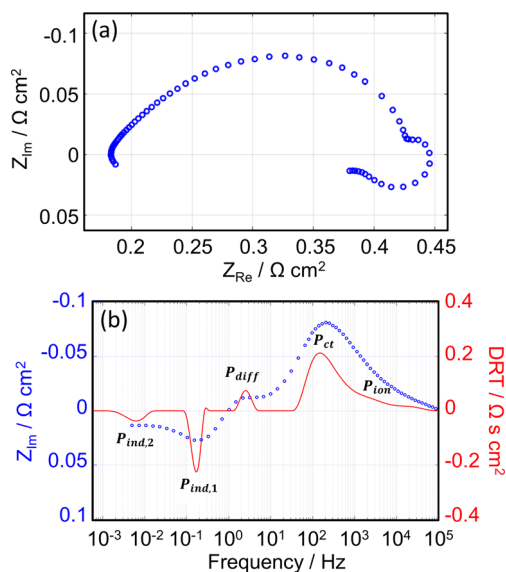nd,2}$, with relaxation frequencies of 200 mHz and 10 mHz, respectively, contributing to the inductive low frequency behavior of the cell. It should be noted that $P_{ind,2}$ is not fully covered in all spectra, as a lower frequency limit of 5 mHz was applied in the measurements.

### 3.3 Equivalent Circuit Model Fitting

An equivalent circuit model (Figure 2a), based on the pre-evaluation of the spectra by the DRT (for details see following chapter), was set up in order to quantify the different polarization contributions. This model is somewhat simplified with respect to the capacitive high frequency processes ($R_1Q_1$, $R_2Q_2$); a more detailed model accounting for microstructural features of the catalyst layer by a transmission line model approach can be found in [16].

Based on [15], two negative RQ elements ($R_3Q_3$, $R_4Q_4$) where the resistances and constant phase elements possess negative values, are used to account for the inductive processes $P_{ind,1}$ and $P_{ind,2}$, respectively. The negative resistance value is thereby understood as a decrease of an ohmic or a polarization resistance exhibiting a higher relaxation frequency. It should be noted that the elements $Q_3$ and $Q_4$ are not related to the physical capacitance of this process but accounting for the dynamics of the decrease in its resistance, which is of course much slower and thus resulting in a very low relaxation frequency. To fit the model to the measured spectra a complex nonlinear least square (CNLS) fitting approach, considering the DRT next to real- and imaginary-part, was chosen [17]. An example for the fitting result is shown in Figure 2b.

# 4 Results and Discussion

### 4.1 Parameter Variations

To analyze the impact of operating parameters on the low-frequency processes, variations of different operating parameters as (i) relative humidity, (ii) current density and (iii) gas composition were performed.
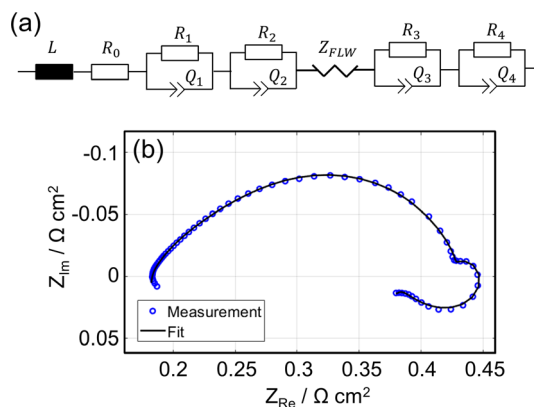


Fig. 1 Impedance spectra measured at 30% R.H., $j = 500\,\text{mA cm}^{-2}$ and $T = 80\,°\text{C}$ (a), and imaginary part as well as the calculated DRT (b).



Fig. 2 Equivalent circuit model describing the impedance spectra including the pseudo-inductive loop at low frequencies ($R_3Q_3$, $R_4Q_4$) (a), and an example for the fitting result of an impedance spectra measured at 30% R.H., $j = 500\,\text{mA cm}^{-2}$ and $T = 80\,°\text{C}$ (b).

### 4.1.1 Variation of Relative Humidity

The water transport characteristic of the membrane and related changes in membrane hydration resulting in conductivity changes, are said to affect the ohmic resistance of the cell and therefore produce an inductive loop [3–5]. To investigate how the hydration of the membrane affects the inductive loop, relative humidity was varied from 30% R.H. to 70% R.H. Other parameters, like temperature ($T = 80\,°C$) and current density ($j = 1,000\,mA\,cm^{-2}$), were kept constant.

In Figure 3a, the Nyquist plot of the spectra reveals that the proportion of the inductive loop is decreasing with increasing relative humidity. In addition, the calculated DRTs in Figure 3b reveal a strongly humidity dependent inductive process $P_{ind,1}$ (~200 mHz), which increases with decreasing humidity. The second inductive process $P_{ind,2}$ (~10 mHz) is only visible for high humidities.

To check the influence of humidity at different current densities, the same variation was carried out at $j = 100\,mAcm^{-2}$. In Figure 4, the comparison of both inductive processes at $j = 100\,mA\,cm^{-2}$ (a) and $j = 1,000\,mA\,cm^{-2}$ (b) is shown.

It becomes evident, that the process $P_{ind,1}$ (100–200 mHz) is nearly independent of the relative humidity for lower current densities while the second process $P_{ind,2}$ (8–20 mHz) varies for different humidities even though no clear dependence is recognizable. At higher current densities $P_{ind,2}$ only occurs with high humidities and $P_{ind,1}$ is clearly dominant at all conditions.

To analyze the impact of water transport in the membrane, measurements with different relative humidities at anode and cathode were performed at 1,000 mA cm$^{-2}$. Water transport is hereby provoked with higher oxidant than fuel humidity. In

**Fig. 4** Detailed view of inductive processes in DRT calculations at $j = 100\,mA\,cm^{-2}$ (a), and $j = 1,000\,mA\,cm^{-2}$ (b) at various relative humidities in oxidant and fuel ranging from 30% R.H. to 70% R.H. ($T = 80\,°C$).

Figure 5a, impedance spectra at 30% R.H. at the anode and two different relative humidities of 30% and 70% at the cathode are given. It becomes evident, that the inductive loop is more pronounced for a similar humidity of 30% at cathode and anode. The DRTs in Figure 5b show, that this behavior is related to $P_{ind,1}$.
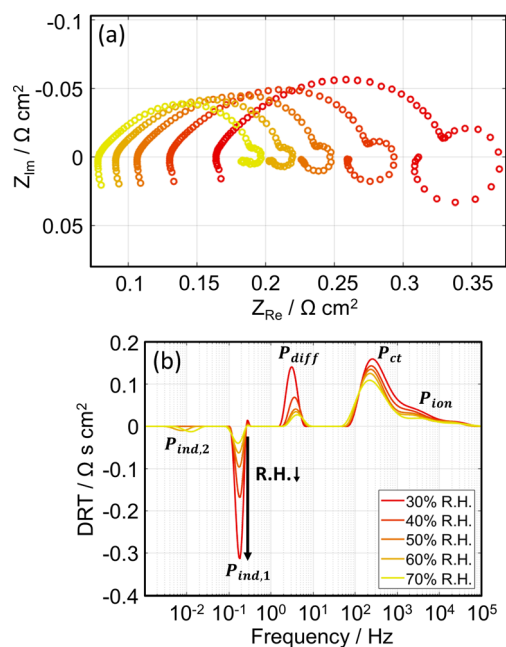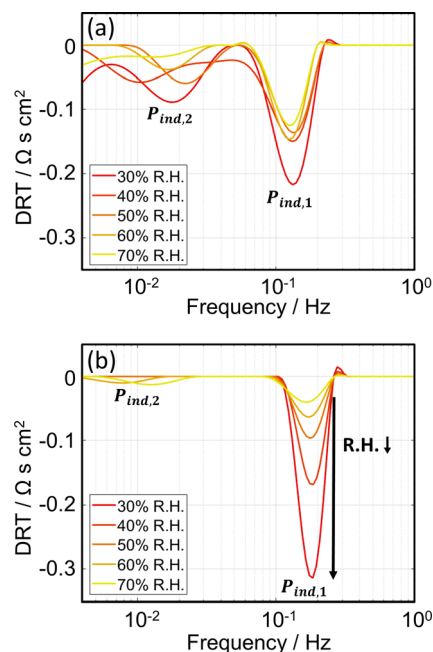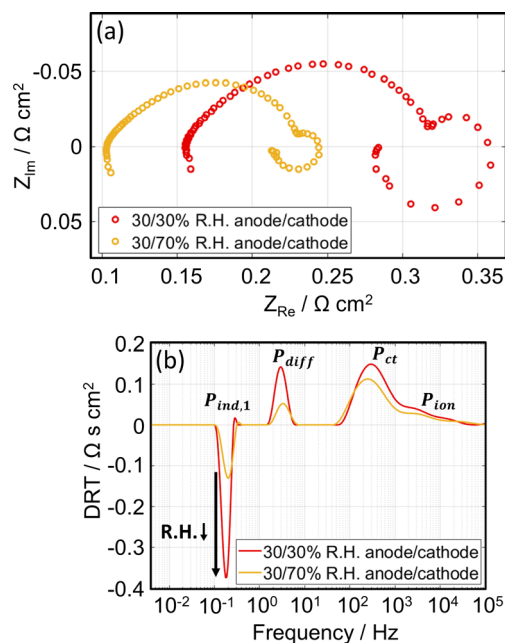
**Fig. 3** Impedance spectra (a), and calculated DRTs (b) at varied relative humidity in oxidant and fuel ranging from 30% R.H. to 70% R.H. ($T = 80\,°C$, $j = 1,000\,mA\,cm^{-2}$).

**Fig. 5** Impedance spectra (a), and calculated DRTs (b) at 30% R.H. at the anode and varied relative humidity (30% and 70% R.H.) at the cathode ($T = 80\,°C$, $j = 1,000\,mA\,cm^{-2}$).

### 4.1.2 Variation of Current Density

Variations of current density at constant relative humidities were performed to investigate the influence of the electrode potential on the inductive loop. Surface effects such as formation of platinum oxide or intermediates in the ORR depend on the surface coverage and thus the potential of the electrode. Both effects are said to be of kinetic nature and an increase in current density results in a slow decrease of the resistance, which will result in a low frequency inductive behavior.

In Figure 6a, impedance spectra measured at various current densities from $50\,mA\,cm^{-2}$ to $900\,mA\,cm^{-2}$ ($T = 80\,°C$, 30% R.H.) are plotted. The overall polarization resistance $R_{pol}$ decreases with increasing current density as expected. The DRTs related to this experiment show the influence of the current density on each polarization process (Figure 6b).

For a more precise analysis of both inductive processes, $P_{ind,1}$ and $P_{ind,2}$, a detailed view of calculated DRTs is given in Figure 7a. $P_{ind,1}$ (100–200 mHz) shows an alternating dependency on the current density: at currents above $300\,mA\,cm^{-2}$ $P_{ind,1}$ increases with increasing current density, whereas the process increases with decreasing current density at currents lower than $100\,mA\,cm^{-2}$. However, this dependency is rather weak and the process remains almost constant. $P_{ind,2}$ (8–20 mHz) decreases with increasing current density and is not visible at $900\,mA\,cm^{-2}$. The overall polarization resistance is larger at lower current densities. However, the process $P_{ind,2}$ is not completely captured in the spectra as the minimum frequency was 5 mHz. Thus, values obtained in the CNLS-fit of the equivalent circuit model might be incorrect.

In order to compare the behavior for a current variation at higher humidities, Figure 7b shows a detailed view of both inductive processes at 70% relative humidity. $P_{ind,2}$ is visible at
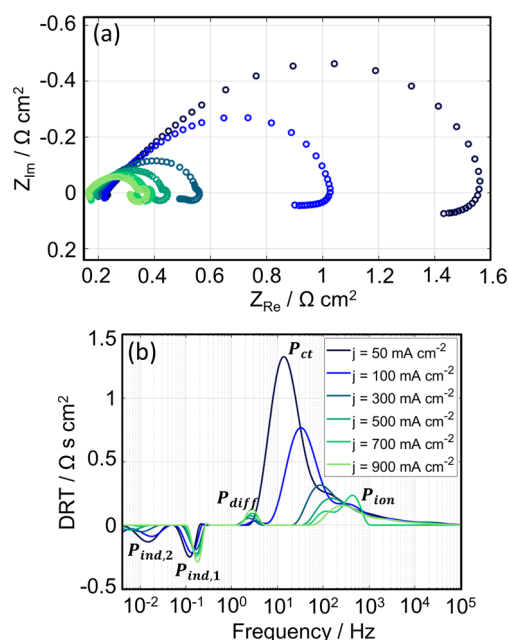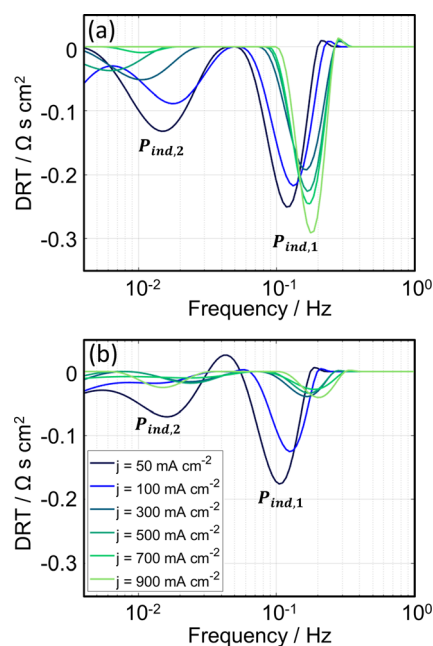


Fig. 7 Detailed view of inductive processes in DRT calculations for 30% R.H. (a), and 70% R.H. (b) at varying current densities from $50\,mA\,cm^{-2}$ to $900\,mA\,cm^{-2}$ ($T = 80\,°C$).

all current densities and further possesses a comparable size to $P_{ind,1}$ at higher current densities.

### 4.1.3 Variation of Gas Composition

In order to investigate the influence of oxygen partial pressure on the observed inductive low-frequency processes, measurements with variations of oxygen partial pressure at different operating conditions were performed. Hereby, mixtures of oxygen and nitrogen were used. It turned out that no clear dependency could be detected.

However, measurements in symmetrical $H_2/H_2$ mode yield to an inductive loop (Figure 8a) but only if a current is applied (i.e., $j = 300\,mA\,cm^{-2}$ and $j = 500\,mA\,cm^{-2}$). The DRT (Figure 8b) again reveals an inductive process $P_{ind,1}$, which is compared to the fuel cell mode approximately one order of magnitude smaller. In open circuit voltage (OCV) measurements ($j = 0\,mA\,cm^{-2}$) no inductive loop was observed.

The fact, that even in absence of oxygen an inductive loop occurs, indicates that the inductive behavior is at least not solely related to intermediates in the oxygen reduction reaction or the formation of platinum oxide. As the effect in the symmetrical $H_2/H_2$ mode is much smaller (a few $m\Omega\,cm^2$ only) it should be related to an additional effect most probably caused by a current-related resistance decay of the hydrogen oxidation/evolution reaction (HOR/HER) polarization resistance. Furthermore, this inductive loop is only visible for current densities $j > 0\,mA\,cm^{-2}$. Thus, the displacement of the system from its equilibrium state (by applying a current) is causing the inductive low-frequency behavior. The DC resistance (real part of the impedance at 5 mHz) is approximately independent of the applied current density and the current
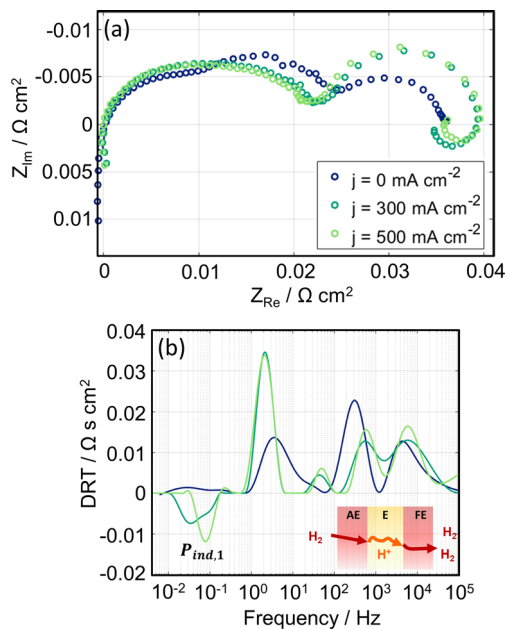


Fig. 6 Impedance spectra (a), and calculated DRTs (b) at varying current densities from $50\,mA\,cm^{-2}$ to $900\,mA\,cm^{-2}$ ($T = 80\,°C$, 30% R.H.).

Fig. 8 Impedance spectra (a), and calculated DRTs (b) in $H_2/H_2$ mode (similar hydrogen partial pressure and humidity of 40% at anode and cathode, $T = 80\,°C$) at OCV and different current densities of $j = 300\ mA\ cm^{-2}$ and $j = 500\ mA\ cm^{-2}$. Ohmic resistances are subtracted for better comparability.

related increase of the capacitive polarization resistance is compensated by the inductive process.

## 4.2 Quantitative Analysis

Considering that the processes $P_{ind,1}$ and $P_{ind,2}$ are caused by a current-related resistance decay [15], i.e., a slow decrease of an ohmic or polarization resistance contribution affected by an increase in current density, the negative area specific resistance (ASR) contributions of these processes and their relation to ohmic and polarization losses of the cell are of interest.

In Figure 9, $P_{ind,1}$ is compared to ohmic resistance $ASR_\Omega$ and the overall polarization resistance related to the sum of the capacitive loss processes $ASR_{pol}$. As the absolute value of the negative $ASR(P_{ind,1})$ even exceeds the ohmic resistance
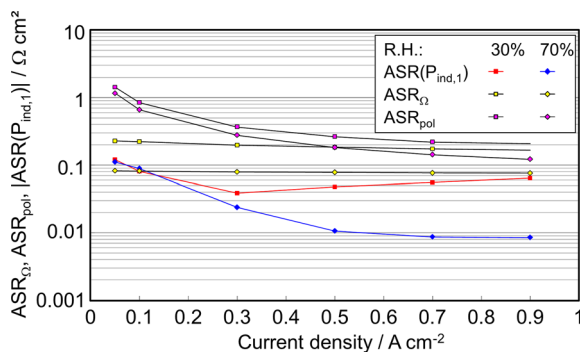
(dominated by the resistance of the membrane) at low current densities, it can be excluded that the impact of water content and transport in the membrane on its conductivity is the (main) cause for the inductive loop. The change of the ohmic membrane resistance caused by the small AC current (<30 mA) applied during the impedance measurements should be in the range of –1 mΩ $cm^2$ only.

In case of the polarization resistance $ASR_{pol}$ similar dependencies are observable and the absolute values of the negative resistances $ASR(P_{ind,1})$ are always below the related $ASR_{pol}$. Thus, it is most likely that one of the polarization processes is affected by a current-related resistance decay [15]. In Figure 10, $ASR(P_{ind,1})$ and $ASR(P_{ind,2})$ are compared to the $ASR_{TLM}$ related to the oxygen reduction in the catalyst layer, which can be described as the interaction of charge transfer- and ionomer-resistance in a transmission line model (TLM) [16].

The quite similar slopes of the curves suggest that at least $P_{ind,1}$ has to be attributed to a current-related resistance decay within the oxygen reduction reaction described by the transmission line model. In case of $P_{ind,2}$ a similar behavior is observed, but it has to be noted that the fitting results are more inexact as this process is not fully covered in the measured spectra.

As platinum oxide formation is favored at high potentials [18], the observed behavior might be correlated to that. However, as the formation of platinum oxide at high current densities – resulting in low cathode potentials – is unusual, a second mechanism related to intermediates (such as $H_2O_2$ [10]) formed in the ORR might be the reason. In both cases the process would be related to electrochemical phenomena at the catalyst surface. Furthermore, it should be noted that an impact of minor amounts of contaminants in the gases might affect the inductive processes.

Figure 11 shows the ratio of the inductive processes $ASR(P_{ind,1}) + ASR(P_{ind,2})$ to the total resistance of the cell (sum of ohmic and polarization resistance $ASR + ASR_{pol}$).This ratio represents a measure for the improvement of the cell due to the inductive processes.
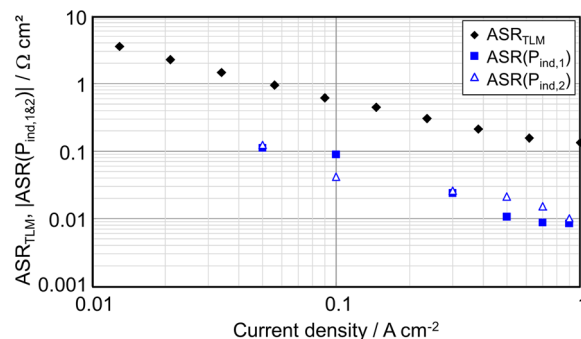


Fig. 9 Comparison of $ASR(P_{ind,1})$ with the ohmic resistance $ASR_\Omega$ and the overall polarization resistance $ASR_{pol}$ displayed for two different relative humidities of 30% and 70%.



Fig. 10 Comparison of $ASR(P_{ind,1})$ with the polarization resistance $ASR_{TLM}$ attributed to the combination of charge transfer reaction and ionic transport in the ionomer (values taken from [16] for 80°C and 70% relative humidity).
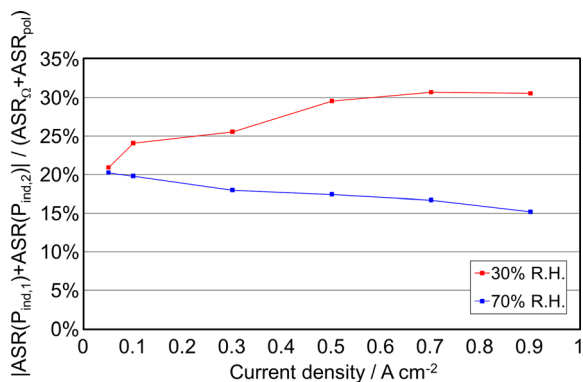
Fig. 11 Ratio of inductive to capacitive and ohmic processes $(ASR(P_{ind,1}) + ASR(P_{ind,2}))/(ASR + ASR_{pol})$ at different current densities and relative humidities.

Table 1 Parameter dependencies and presumable physical origins of inductive polarization processes.

|  | $P_{ind,1}$ (100–200 mHz) | $P_{ind,2}$ (10–20 mHz) |
|---|---|---|
| **Parameter dependency** | | |
| Current density | low | strong |
| Relative humidity | strong | low |
| $pO_{2,cathode}$ | no dependency | no dependency |
| $pH_{2,sym.}$ | visible/identifiable | not identifiable |
| **Physical origin** | | |
| Membrane conductivity | no | no |
| PtO at high potential | possible | possible |
| Intermediates (ORR) | possible | possible |
| HOR/HER | yes (only minor contribution) | no |

The observed values are in a range from 15% to 30%. Thus, a considerable impact of the inductive low-frequency processes on the cell performance has to be taken into account.

Table 1 summarizes the dependencies and presumable origins of the inductive processes.

## 5 Conclusions

In this study, an extended version of the distribution of relaxation times (DRT) has been implemented and applied to study inductive low-frequency processes in impedance spectra of PEMFCs. By a systematic variation of operating parameters performed on a lab-scale (1 cm$^2$) commercial MEA, information about operating parameter dependencies and possible physical origins were revealed.

In the DRT two inductive processes $P_{ind,1}$ and $P_{ind,2}$, with relaxation frequencies of 100 to 200 mHz and 8 to 20 mHz respectively, could be determined. An extended equivalent circuit model describing those processes by negative resistances and constant phase elements was set up to quantify the inductive low-frequency processes.

Both inductive processes are depending on relative humidity and current density. Whereas $P_{ind,2}$ is strongly decreasing

with increasing current density, the current density dependency of $P_{ind,1}$ depends on the relative humidity. The inductive behavior seems to be dominated by the ORR at the cathode and processes as platinum oxide formation and intermediates formed in the ORR might be the reason for the observed behavior. Water formation and transport related changes in membrane hydration can be excluded as the main cause for the inductive low-frequency processes. Furthermore, it was observed that the inductive processes $P_{ind,1}$ can be observed in the symmetrical $H_2/H_2$ mode to a minor extend. Thus, the observed process cannot be solely related to the ORR.

The analysis of the inductive low-frequency behavior showed that a single physical mechanism is not sufficient to explain the observed parameter dependencies and that at least 3 different mechanisms should be considered in a comprehensive model. To set up such model and clearly correlate the inductive low-frequency processes to their physical origins further measurements including variations in cell parameters as Pt-loading and catalyst layer thickness should be performed. Based on this knowledge, targeted measures to increase the absolute values of the negative polarization resistances, which will improve the cell performance, can be developed.

## References

[1] B. P. Setzler, T. F. Fuller, *J. of Electrochemical Society* **2015**, *162*, F519.

[2] S. K. Roy, M. E. Orazem, B. Tribollet, *J. of Electrochemical Society* **2007**, *154*, B1378.

[3] G. Futter, P. Gadzdzicki, K. Friedrich, A. Latz, T. Jahnke, *J. Power Sources* **2018**, *391*, 148.

[4] N. Holmström, K. Wiezell, G. Lindbergh, *J. of Electrochemical Society* **2012**, *159*, F369.

[5] I. A. Schneider, M. H. Bayer, A. Wokaun, G. G. Scherer, *J. of Electrochemical Society* **2008**, *155*, B783.

[6] I. Pivac, F. Barbir, *J. Power Sources* **2016**, *326*, 112.

[7] E. Ivers-Tiffée, A. Weber, *J. of the Ceramic Society of Japan* **2017**, *125*, 193.

[8] M. Heinzmann, A. Weber, E. Ivers-Tiffée, *J. Power Sources* **2018**, *402*, 24.

[9] A. Leonide, V. Sonn, A. Weber, E. Ivers-Tiffée, *J. of Electrochemical Society* **2008**, *155*, B36.

[10] B. A. Boukamp, *J. of Electrochemical Society* **1995**, *142*, 1885.

**ORIGINAL RESEARCH PAPER**

[11] M. Schönleber, D. Klotz, E. Ivers-Tiffée, *Electrochimica Acta* **2014**, *131*, 20.

[12] H. Schichlein, A. C. Müller, M. Voigts, A. Krügel, E. Ivers-Tiffée, *J. of Applied Electrochemistry* **2002**, *32*, 875.

[13] A. Tikhonov, A. Goncharsky, V. Stepanov, A. Yagola, *Numerical Methods for the Solution of Ill-Posed Problems*, Kluwer Academic Publishers, Dordrecht, Boston, London, **1990**.

[14] J. Weese, *Computer Physics Communications* **1992**, *69*, 99.

[15] D. Klotz, *Electrochemistry Communications* **2019**, *98*, 58.

[16] M. Heinzmann, A. Weber, E. Ivers-Tiffée, *J. Power Sources* **2019**, *444*.

[17] D. Klotz, J. P. Schmidt, A. Kromp, A. Weber, E. Ivers-Tiffée, *ECS Transactions* **2012**, *41*, 25.

[18] S. Arisetty, Y. Liu, W. Gu, M. F. Mathias, *ECS Transactions* **2015**, *69*, 273.